An investigation of polar ozone recovery in the 1997 Southern Hemisphere spring

J. M. Pierson

Universities Space Research Association

A. R. Douglass, S. R. Kawa, and P. A. Newman

NASA Goddard Space Flight Center

Short title:

Abstract.

A chemical transport model is used to investigate the processes that control the depth and duration of the ozone 'hole' in the lower stratosphere through comparisons of model output with measurements from the Total Ozone Mapping Spectrometer (TOMS) and from the Microwave Limb Sounder (MLS) and Halogen Occultation Experiment (HALOE), both on the Upper Atmosphere Research Satellite (UARS). This study extends previous model comparisons with observations into October and November and examine levels in (>31 hPa) and above (<31 hPa) the chemical loss region. Averages of column ozone in the model decrease through mid-October below 31 hPa but begin to increase in mid-September above 31 hPa. An investigation of model-tracer data comparisons and other meteorological parameters indicate that the model presents a consistent picture of top-down recovery and tracer transport. An O_3 budget study at 500 K (below 31 hPa) and 840 K (above 31 hPa) is carried out to investigate the processes that control the timing of the transition of ozone from a chemical to dynamically driven regime. The model ozone decrease at 500 K is due to chemical loss in August and September but is due to upward motion in October. The ozone increase at 840 K is primarily due to photochemical production, with a smaller contribution from transport. These results show that chemistry and dynamics can play different roles in polar vortex ozone recovery at different levels.

Introduction

Models simulating ozone behavior must have the appropriate balance of dynamics, photochemistry and radiative processes to mimic the response of ozone in the stratosphere to natural and anthropogenic changes. Model performance is evaluated by demonstrating that model output is similar to observations from satellites, balloons and aircraft. This approach has been applied to investigating stratospheric Arctic and Antarctic ozone loss during the winter and early spring. Three-dimensional models with assimilated winds and temperatures have been used successfully to evaluate the timing of chlorine activation by polar stratospheric clouds (PSCs), and the relative contribution of different ozone loss mechanisms during the Arctic winter [*Chipperfield et al.*, 1994a; *Chipperfield et al.*, 1994b; *Lefevre et al.*, 1994; *Lefevre et al.*, 1998; *Chipperfield and Pyle*, 1998; *Hansen and Chipperfield*, 1999; *Goutail et al.*, 1999; *Douglass et al.*, 1993; *Deniel et al.*, 1998]. A year by year study using meteorological input from the European Center for Midrange Weather Forecasting [*Chipperfield et al.*, 1996a] and a multi-year simulation of the polar winter using UKMO input [*Chipperfield*, 1999] have shown that interannual variability in meteorology does have an affect on the potential for ozone loss. Modeling studies of the Arctic and Antarctic winter/spring have been able to define the altitude range of greatest ozone loss (400-500 K) but underestimate the cumulative loss in this region [*Chipperfield et al.*, 1996b; *Ricaud et al.*, 1998; *Deniel et al.*, 1998]. These model studies focused primarily on the time and altitude region of greatest ozone loss but do not consider the interplay between chemistry and dynamics and the role each

has throughout more of the vortex.

In this study of the 1997 Antarctic winter and early spring, we extend model comparisons with observations into October and early November and examine levels in and above the chemical loss region. Previous Antarctic model studies have examined the time period between August and September and between the 450 K and 600 K potential temperature surfaces inside the vortex [*Chipperfield et al.*, 1996b; *Ricaud et al.*, 1998]. Photochemistry and dynamics, however, continue to influence the depth and duration of the ozone 'hole' beyond September. The 3D CTM is a tool which can be used to compare constituent evolution with observations to evaluate what processes control ozone in transitioning from a chemical to transport driven regime. Understanding how these processes control ozone is important if we are to assess future impacts of changing chlorine levels and climate change on ozone.

This paper presents general vortex chararcteristics for the 1997 Southern Hemisphere from August to November 1997 in the lower stratosphere. The observations are described in the next section. Section 3 describes the 3D CTM. In Section 4, comparisons of total column observations from the Earth Probe Total Ozone Mapping Spectrometer (TOMS) with model fields show that the model total column is within 15% of the TOMS observations and consistent with the observed ozone column tendency. Separating the model column into layers shows that the column increases above 31 hPa beginning in mid-September but decreases through early October below 31 hPa. Meteorological fields at 500 K and 840 K chosen to represent these regions and comparisons with methane observations from the Halogen Occultation Experiment

(HALOE) demonstrate that the model dynamics produce a consistent picture of vortex evolution and strength providing confidence in the model dynamics. In Section 5, we compare vortex averaged O_3 with observations from the Microwave Limb Sounder (MLS) at 500 K and 840 K, to show that the modeled ozone evolution agrees fairly well with observations and is consistent with the model column behavior. Using the model ozone tendency, model production, and model loss terms, we show that the ozone decrease at 500 K in August and September is due to chemical loss but is the result of upward motion in October. At 840 K, photochemical production is mainly responsible for the ozone increase beginning in mid-September. Section 6 provides a summary of the results.

2. Data

The constituent fields in the CTM will be compared with observations from MLS, HALOE (both on UARS) and TOMS. The MLS views from 34 degrees latitude in one hemisphere to 80 degrees latitude in the other hemisphere for periods of about a month, during which the satellite orbit precesses. The spacecraft is then yawed to keep the cold side away from the Sun, and MLS views the opposite hemisphere. Power limitations on UARS reduce MLS coverage of the Southern Hemisphere winter to scattered days during August, September, October and November 1997. HALOE makes observations at each of two latitudes most days during the winter; the scan pattern sweeps with time, to obtain near global coverage in about one month. TOMS provides observations for the sunlit portion of the Earth on a daily basis. Each instrument is described below.

using the version 18 algorithm. It is estimated that the total error for 50 to 0.3 hPa is less than 15% with a precision of 7% or less.

Total Ozone Mapping Spectrometer (TOMS)

The Earth Probe TOMS instrument provides measurements of total column ozone by measuring solar irradiance and the radiance backscattered by the Earth's atmosphere in six selected wavelength bands in the ultraviolet [*McPeters, et al.*, 1998]. Retrieval of total ozone is based on the comparison between measured normalized radiances and radiances derived by radiative transfer calculations for different ozone amounts. The algorithm is identical to the one used for the Version 7 Nimbus-7 and Meteor-3 TOMS. For Earth Probe TOMS, the absolute error is 3%, random error is 2%, and drift is less than 0.6%.

3. GSFC Chemistry and Transport Model

The CTM used here is an improved version of that used in previous analyses of observations from UARS instruments MLS, the Cyrogenic Limb Array Etalon Spectrometer (CLAES), and HALOE [*Kawa et al.*, 1995; *Douglass et al.*, 1997; *Douglass and Kawa,* 1999] and NIMBUS 7 TOMS observations [*Douglass et al.*, 1996]. The assimilation system is fully described by Data Assimilation Office (DAO) [1997]. *Douglass and Kawa* [1999] discuss the improvements to the assimilation system resulting from the rotation of the computational pole to the equator and raising the top level of the general circulation model from 0.4 hPa to 0.1 hPa in the assimilation.

The assimilation fields are produced at 2° latitude by 2.5° longitude horizontal resolution and are used on this horizontal grid in the CTM. There are a lot more levels in the assimilation than in the model. The assimilation winds are mapped onto the model vertical levels using an integration scheme developed by S. J. Lin (personal communication, 1999). There are 28 model vertical levels, with 11 sigma levels in the lower atmosphere and 17 pressure levels above with a boundary at 130 hPa separating the sigma and pressure regimes. The spacing is about 1.5 km up to 20 km, and increases to 4 km above 30 km. Advection is accomplished using the transport scheme developed by *Lin and Rood* [1996].

The photochemical scheme, calculated in 15 minute timesteps, includes all gas phase reactions thought to be important in the stratosphere; rate constants and temperature-dependent cross sections are taken from *DeMore et al.* [1994]. Changes in recommended values for some of the gas phase reactions as reported in *DeMore et al.* [1997] are not important to this study. The heterogeneous chemistry package (reactions, surfaces, surface areas, particle size and sticking coefficients) is described by *Douglass and Kawa* [1999] and is essentially identical to the recommendation by *DeMore et al.* [1997] but does not include sedimentation, denitrification or dehydration.

For all simulations, the initialization for long-lived species and families follows the procedure described by *Douglass et al.* [1997]. The simulation is initialized March 18, 1997 and continues until March 18, 1998. Since the model study period does not begin until August 1, 1997, there is little or no sensitivity to the initial conditions.

4. Results

Ozone column and vortex characteristics

Figure 1 shows the time series of the vortex average total column ozone from TOMS and the model from August 1 to mid-November. The vortex edge at 500 K is defined to be the location of the highest Ertel's potential vorticity (EPV) gradient [*Nash et al.*, 1996]. Both the model and the TOMS total column decrease from September 1 to early October. The model total column is within 15% of the TOMS column during this period and is in better agreement as the column levels off in mid-October. This difference, however, is not the result of a difference in the way the model and TOMS sample the vortex. The model captures the rapid increase in the total column seen in the TOMS observations as the vortex begins to break up in mid-November.

We separate the model total ozone column to examine the column tendency at different levels. The column below 57 hPa decreases from August through early October then levels off. The column between 31 and 57 hPa exhibits similar behavior. Above 31 hPa, however, the column begins to increase in mid to late September. Figure 1 shows that the increase above 31 hPa contributes about 10 DU to the column change between mid-September and mid-October. We focus our investigation on the 31-57 hPa and above 31 hPa regions by examining the vortex at 500 K (approximately 40 hPa) and 840 K (approximately 10 hPa).

The modified potential vorticity (MPV) [*Lait*, 1994] for the 500 K potential temperature surface in the Southern Hemisphere from August 1 to November 15 shows

that the vortex remains well-defined up to November 15 (Figure 2). MPV intensifies near the pole in September. The intensity of the vortex remains nearly constant until November 1, after which the vortex weakens (see November 15) and breaks up around November 20 (not shown). The MPV on the 840 K surface is shown in Figure 3. The shape of the vortex at 840 K is very similar to the shape at 500 K, but the evolution differs. While the vortex strengthens through September on the 500 K surface, the vortex at 840 K begins weakening in September, and the maximum horizontal gradient, which locates the boundary separating the vortex and middle latitudes, decreases much more quickly.

We use a study similar to *Newman* [1986] to define the final warming and vortex breakdown on the 500 K and 840 K potential temperature surfaces. *Labitzke and Van Loon* [1972] described the transition from winter to summer as a reversal of the pole to mid-latitude temperature difference. *Miller et al.* [1970] and *Yamazaki et al.* [1985] found that the reversal in pole to mid-latitude temperature gradient is followed by a decrease in the zonal mean wind to weak westerlies or reversal to weak easterlies. Figure 4 shows the analyzed average wind speed at the vortex edge on the 500 and 840 K potential temperature surfaces. At 840 K, the average wind speed at the vortex edge remains fairly constant until early October when it begins to decrease at a rate of 1 m/s/day. Wind speeds along the vortex edge at 500 K however remain constant until November before falling off at a similar rate. Figure 5 shows that the difference between the zonal average temperature at 82°S and 50°S changes sign in early October at 840 K but not until mid-November at 500 K. Both of these diagnostics along with the MPV

plots in Figure 2 and 3 are consistent with top-down recovery; the vortex weakens first at the higher altitudes and we expect to see an increase in ozone mixing ratios as higher ozone air moves into the vortex from mid-latitudes. The jumps in the temperature differences for both surfaces in mid-October and early November are related to vortex wobble.

Comparisons between observed and modeled constituents provide a means to assess chemistry and transport in the model. Figure 6 compares the modeled CH_4 with HALOE sunset profiles from October 1, 1997. The contour plot of model CH_4 at 15 mb (Figure 6a) shows a distinct gradient between vortex and mid-latitude air, with higher values of CH_4 outside the vortex than inside the vortex. The locations of the HALOE sunset profiles are shown in Figure 6a (asterisks), and Figure 6b displays these data as functions of pressure. Figure 6c shows the modeled CH_4 profiles closest in time and space to the HALOE profiles. The profiles in Figure 6b and 6c are color-coded to match the CH_4 mixing ratios seen in Figure 6a. The HALOE and model profiles both show CH_4 increasing with increasing pressure. The horizontal structure observed in HALOE CH_4 is consistent with that in the model field. Both show differences in the shapes of vortex and mid-latitude profiles. The weak vertical gradient in HALOE CH_4 between 1 and 15 hPa in the vortex is similar to that reported by *Russell et al.* [1993b] and results from descent of mesospheric air from above [*Fisher et al.*, 1993]. In the model, a weak vertical gradient is produced between 1 and 10 hPa. At 15 hPa, the difference between a HALOE vortex and midlatitude profile is about 0.8 ppmv CH_4 but only 0.4 ppmv CH_4 in the model. Part of the discrepancy between the model and HALOE is due to the lack

of a model mesosphere, as there are no CH_4 mixing ratios as small as those observed by HALOE at 1 hPa during winter anywhere in the model domain. Below 10 hPa, the differences are a result of insufficient descent or too vigorous meridional mixing in the model. In general, the model simulates the structure and evolution of the trace gas distribution in the high-latitude spring fairly well so that we may focus our attention on O_3 and the interplay of chemistry and dynamics.

5. Ozone tendency at different levels

To identify the processes contributing to the ozone evolution in the model, we focus on the 500 and 840 K potential temperature surfaces. Figure 7 provides a comparison of timeseries for these two surfaces for the model ozone (Figures 7a and 7b), the model ozone tendency (Figures 7c and 7d), the net photochemical production, loss, and their sum (Figures 7e and 7f), and lastly, the contribution to the ozone tendency from advection (Figures 7g and 7h) determined from the continuity equation

$$\partial O_3/\partial t = P + L + \text{Advection} \quad (1)$$

where $\partial O_3/\partial t$ is the ozone tendency, P is model ozone production and L is the model ozone loss. All of these quantities are area-weighted vortex averages.

Figure 7a directly compares the area-weighted model vortex average O_3 mixing ratio (solid lines) with symbols which represent the MLS area-weighted O_3 vortex average. The model average ozone mixing ratio at 500 K decreases from 3.5 to 1 ppmv

from August 1 through November 1 and agrees with the MLS O_3 vortex averages found in early August and late October but agreement is poorer in late August and early October. The poorer agreement is most likely the result of not having denitrification and sedimentation in the model. Figure 7c shows that the change in O_3 at 500 K is on the order of -0.02 to -0.03 ppmv/day, consistent with previous studies in the Antarctic [*McKenzie et al.*, 1996]. Figure 7e shows the change in ozone due to chemistry from the area-weighted vortex average O_3 production and loss. At 500 K, the decrease in ozone between August and September is primarily the result of chemical loss of ozone by activated chlorine. As polar night recedes and sunlight returns to the region, production begins to offset the effects of the loss processes, and eventually the chemical tendency in ozone is positive (although very small) as active chlorine decreases through reformation of chlorine reservoirs. Advection, however, contributes more to the ozone tendency in October than photochemical processes (Figure 7g).

There are several pieces of information that support advection being the source of ozone loss in late October and early November. Although the effects of not having denitrification and sedimentation in the model are apparent in the model-data comparisions in late August and mid-October, *Brasseur et al.* [1997] demonstrated using a model that denitrification and sedimentation have little impact on ozone loss in late October and early November. Model N_2O fields on the 500 K surface do not increase in August and September but increase through all of October and into November (not shown). Horizontal advection at 500 K would increase O_3 and N_2O while downward motion would decrease N_2O. Upward motion, which decreases O_3 and increases N_2O,

describes the model ozone tendency. Calculations by *Rosenfield and Schoeberl* [1999] using diabatic heating rates and trajectories for 1997 show weak descent within the vortex up to September 1 but upward motion by October 1. As the vortex experiences increased insolation, increased radiative heating results in upward motion. Finally, a model study by *Lefevre et al.* [1998] for the 1996-1997 Arctic winter also showed that a large-scale dynamics induced minimum contributed to the anomalously low columns over the Arctic in March [*Newman et al.*, 1997] along with chemical loss.

Figure 7b shows that at 840 K the model O_3 mixing ratio remains unchanged at about 4 ppmv through early September and increases to 4.75 ppmv by mid-October. This change is also seen in the MLS observations. Figure 7d shows that ozone increases in September at a rate of 0.02-0.04 ppmv/day. Comparing figure 7d with 7f and 7h shows that the increase in model ozone between September and early October is primarily due to chemical production (Figure 7f). Note the production and loss curves are scaled down by a factor of 5 to fit the same scale as Figures 7d and 7h, consistent with higher photolysis rates at higher altitudes. Figure 7h indicates that advection does contribute to the September-early October model ozone increase with more of a contribution in the early part of September, but photochemical production plays the larger role at 840 K.

Manney et al. [1993] point out that planetary wave activity generally increases in August and September leading to more transport and more distortion and changes in vortex size. To further illustrate the importance of photochemistry to the O_3 increase at 840 K during September and early October, we plot the vortex edge and O_3 as a function of equivalent latitude in Figure 8. The white solid line denotes the equivalent

latitude of the vortex edge. Through most of August, the area of the vortex ranges between an equivalent latitude of 54°S to 62°S . For September and early October, however, the vortex boundary remains constant at 62°S . Thus, the increase in model ozone at 840 K in Figure 7b is not an artifact of horizontal advection across the vortex edge or a change in the vortex size. Figure 8 also shows that the increase in model ozone occurs throughout most of the vortex and is consistent with the calculations in Figure 7 (b,d,f,h).

6. Summary and Conclusions

The results presented here, which document the 1997 Southern Hemisphere late winter and early spring as part of a one year model simulation using assimilated winds, were used to clarify the processes that control the depth and duration of the 1997 Antarctic ozone 'hole'. Separating the model column into different levels showed that the tendency of the total ozone column does not reflect the tendency at all levels. While the model total column is fairly constant in October, the column above 31 hPa is increasing but the column below 31 hPa is decreasing. Designating 500 K and 840 K theta levels to represent these regions, an investigation of modified potential vorticity, assimilated winds, and assimilated temperatures at these levels show that the model presents a consistent picture of the vortex weakening from above leading to ozone recovery from the top down. Model-tracer data comparisons of CH_4 profiles also showed that the model has reasonable tracer transport, lending further support to the model dynamics. Using the ozone continuity equation, model production, and loss, the

processes responsible for the ozone tendency at each level were identified:

• Area weighted vortex averages of model and MLS O_3 at 500 K both show that ozone decreases from August through the end of October. The decrease in August and September is due to chemical loss. The loss in October, however, is the result of upward motion due to heating as sunlight returns to high latitudes. A year by year investigation of the heating rates and trajectories shows that the uplift at 500 K does occur in other years but not every year (J. Rosenfield, personal communication, 1999).

• At 840 K, both the model and UARS measurements exhibit an increase in the ozone mixing ratio during September and early October. Advection and mixing contribute to the September-early October model ozone increase but photochemical production is dominant during most of the period.

These results show that the recovery of the 1997 ozone 'hole' is a mixture of chemistry and dynamics at different altitudes and not solely one process or the other. At higher altitudes (840 K) after November 1, dynamics do represent the main process for ozone increases (not shown here). It is important to recognize, however, that the initial recovery of ozone in 1997 is due to photochemical production. Likewise, the ozone decreases in late October and November at 500 K are not chemical but dynamical. This study shows that both chemistry and dynamics can play unique roles to influence the depth and recovery of the ozone hole and it is important to understand their roles as chlorine levels continue to level off and the climate change plays an increasing role defining meteorological conditions.

References

Barath, F., et al., The upper atmosphere research satellite microwave limb sounder instrument, *J. Geophys. Res., 98*, 10751-10762, 1993.

Brasseur, G., et al., A three-dimensional simulation of the Antarctic ozone hole: Impact of anthropogenic chlorine on the lower stratosphere and upper stratosphere, *J. Geophys. Res., 102*, 8909-8930, 1997.

Chipperfield, M., D. Cariolle, and P. Simon, A 3-dimensional transport study of PSC processing during EASOE, *Geophys. Res. Lett, 21*, 1463-1466, 1994a.

Chipperfield, M., D. Cariolle, and P. Simon, A 3-dimensional study of chlorine activations during EASOE, *Geophys. Res. Lett, 21*, 1467-1470, 1994b.

Chipperfield, M., A. M. Lee, J. A. Pyle, Model calculations of ozone depletion in the Arctic polar vortex for 1991/1992 to 1994/1995, *Geophys. Res. Lett, 23*, 559-562, 1996a.

Chipperfield, M. P., et al., Analysis of UARS data in the southern polar vortex in September 1992 using a chemical transport model, *J. Geophys. Res., 101*, 18861-18881, 1996b.

Chipperfield, M., and J. A. Pyle, Model sensitivity studies of Arctic ozone depletion calculations of ozone depletion in the Arctic, *J. Geophys. Res., 103*, 28389-28403, 1998.

Chipperfield, M. P., Multiannual simulation with a three dimensional chemistry transport model, *J. Geophys. Res., 104*, 1781-1805, 1999.

DAO, Algorithm Theoretical Basis Document Version 1.02, Data Assimilation Office, NASA Goddard Space Flight Center, 1997.

DeMore, W. B., et al., Chemical kinetics and photochemical data for use in stratospheric modeling, *JPL Publication 94-20*, NASA, 1994.

DeMore, W. B., et al., Chemical kinetics and photochemical data for use in stratospheric modeling, *JPL Publication 97-4*, NASA, 1997.

Deniel, C., R. M. Bevilacqua, J. P. Pommereau, and F. Lefevre, Arctic chemical ozone depletion during the 1994-1995 winter deduced from POAM II satellite observations and the REPROBUS three-dimensional model, *J. Geophys. Res., 103*, 19,231-19,244, 1998.

Douglass, A. R., R. B. Rood, J. W. Waters, L. Froidevaux, W. Read, L. Elson, M. Geller, Y. Chi, M. C. Cerniglia, and S. Steenrod, A 3D simulation of the early winter distribution of reactive chlorine in the north polar vortex, *Geophys. Res. Lett., 20*, 1271-1274, 1993.

Douglass, A. R., C. J. Weaver, R. B. Rood and L. Coy, A three dimensional simulation of the ozone annual cycle using winds from a data assimilation system, *J. Geophys. Res., 101*, 1463-1474, 1996.

Douglass, A. R., R. B. Rood, S. R. Kawa, and D. J. Allen, A three dimensional

simulation of the middle latitude winter ozone in the middle stratosphere, *J. Geophys. Res., 102*, 19,217-19,232, 1997.

Douglass, A. R. and S. R. Kawa, Contrast between 1992 and 1997 high-latitude spring Halogen Occultation Experiment observations of lower stratospheric HCl, *J. Geophys. Res., 104*, 18739-18754, 1999.

Fisher, M., A. O'Neill, and R. Sutton, Rapid descent of mesospheric air into the stratospheric polar vortex, *Geophys. Res. Lett., 20*, 1267-1270, 1993.

Froidevaux, L., et al., Validation of UARS Microwaves Limb Sounder ozone measurements, *J. Geophys. Res., 101*, 10,017-10,060, 1996.

Goutail, F., et al., Depletion of column ozone in the Arctic during the winters of 1993-1994 and 1994-1995, *J. Atm. Chem., 32*, 1-34, 1999.

Hansen, G. and M. P. Chipperfield, Ozone depletion at the edge of the Arctic polar vortex 1996-1997, *J. Geophys. Res., 104*, 1837-1845, 1999.

Kawa, S. R., J. B. Kumer, A. R. Douglass, A. E. Roche, S. E. Smith, F. W. Taylor, and D. J. Allen, Missing chemistry of reactive nitrogen in the upper stratospheric polar winter, *Geophys. Res. Lett., 22*, 2629-2632, 1995.

Labitzke, K., and H. Van Loon, The stratosphere in the Southern Hemisphere, *Met. Mono., 13*, 113-138, 1972

Lait, L. R., An alternative form for potential vorticity, *J. Atm. Sci., 51*, 1754-1759, 1994.

Lefevre, F., G. P. Brasseur, I. Folkins, A. K. Smith, and P. Simon, Chemistry of the 1991-1992 stratospheric winter: Three dimensional model simulations, *J. Geophys. Res., 99*, 8183-8197, 1994.

Lefevre, F., F. Figarol, K. S. Carslaw, T. Peter, The 1997 Arctic ozone depletion quantified from 3-dimensional model simulations, *Geophys. Res. Lett., 25*, 2425-2428, 1998.

Lin, S. J., and R. B. Rood, Multidimensional flux form semi-Lagrangian transport schemes, *Mon. Wea. Rev., 124*, 2046-2070, 1996.

Manney, G. L., L. Froidevaux, J. W. Waters, L. S. Elson, E. F. Fishbein, R. W. Zurek, R. S. Harwood, and W. A. Lahoz, The evolution of ozone observed by UARS MLS in the 1992 late winter southern polar vortex, *Geo. Res. Lett., 20,* 1279-1282, 1993.

McKenzie, I. A., R. S. Harwood, L. Froidevaux, W. G. Read, J. W. Waters, Chemical loss of polar vortex ozone inferred from UARS MLS measurements of ClO during the Arctic and Antarctic winters of 1993, *J. Geophys. Res., 101*, 14505-14518, 1996.

McPeters, R., et al., Earth Probe Total Ozone Mapping Spectrometer Data Product User's Guide, *NASA Technical Publication 1998-206895*, November 1998.

Miller, A. J., F. G. Finger, M. E. Gelman, 30mb synoptic analyses for the 1969 Southern Hemisphere winter derived with the aid of NIMBUS III (SIRS) data, *NASA TM X-2109*, 1970.

Nash, E. R., P. A. Newman, J. E. Rosenfield, and M. R. Schoeberl, An objective determination of the polar vortex using Ertel's potential vorticity, *J. Geophys. Res., 101*, 9471-9478, 1996.

Newman, P. A., The final warming and polar vortex disappearance during the Southern Hemisphere spring, *Geophys. Res. Lett., 13*, 1228-1231, 1986.

Newman, P. A., et al., Anomalously low ozone over the Arctic, *Geophys. Res. Lett., 13*, 2689-2692, 1997.

Park, J. H., et al., Validation of Halogen Occultation Experiment CH_4 measurements from the UARS, *J. Geophys. Res., 101*, 10183-10203, 1996.

Ricaud, P., et al., Stratosphere over Dumont d'Urville, Antarctica, in winter 1992, *J. Geophys. Res., 103*, 13267-13284, 1998.

Rosenfield, J. E. and M. R. Schoeberl, Investigations of polar descent in the Antarctic, POAM Science Meeting, Berkeley Springs, WV, Oct. 20-22, 1999.

Russell, J. M. III, L. L. Gordley, J. H. Park, S. R. Drayson, A. F. Tuck, J. E. Harries, R. J. Cicerone, P. J. Crutzen and J. E. Frederick, The Halogen Occultation Experiment, *J. Geophys. Res., 98*, 10,777-10,797, 1993a.

Russell, J. M., III, A. F. Tuck, L. L. Gordley, J. H. Park, S. R. Drayson, J. E. Harries, R. J. Cicerone, and P. J. Crutzen, HALOE Antarctic observations in the spring of 1991, *Geophys. Res. Lett., 20*, 719-722, 1993b.

Yamazaki, K. and C. R. Mechoso, Observations of the final warming in the stratosphere of the Southern Hemisphere during 1979, *J. Atmos. Sci.*, *42*, 1198-1205, 1985.

Received _____

Figure 1. Area-weighted vortex column averages based on vortex edge at 500 K. Solid line represents model total column ozone, long dashed line represents TOMS total column ozone, short dashed line represents model column below 57 hPa, dash-dot line represents model column between 31 and 57 hPa and dash-dot-dot line represents model column above 31 hPa.

Figure 2. Modified potential vorticity from the assimilation on the 500 K surface.

Figure 3. Modified potential vorticity from the assimilation on the 840 K surface.

Figure 4. Time series from September 1 to December 1, 1997 of model average wind at vortex edge on the 500 and 840 K potential temperature surfaces.

Figure 5. Time series from September 1 to December 1, 1997 of temperature gradient between 82 and 50°S as seen in the model on the 500 and 840 K potential temperature surfaces.

Figure 6. Model versus observed CH_4 from HALOE sunset measurements on October 10, 1997; (a) Contour plot of the Southern Hemisphere model CH_4 with the position of the HALOE profiles denoted by asterisks; (b) Corresponding HALOE CH_4 profiles marked in (a); (c) Nearest model CH_4 profiles. Profiles in 6b and 6c are color coded to match the model CH_4 mixing ratios at 15 hPa in Figure 6a.

Figure 7. (a) Time series of area-weighted model vortex average O_3 at 500 and (e) 840 K between August 1 and November 1, 1997; (b,f) Change in ozone mixing ratio with respect to time ($\partial O_3/\partial t$, ppmv/day); (c,g) change in ozone mixing ratio due to chemistry ($\partial O_3/\partial t$, ppmv/day). Production and loss curves have been scaled down by a factor of 5; (d,h) change in the ozone mixing ratio due to advection ($\partial O_3/\partial t$, ppmv/day)

Figure 8. Contour plot of timeseries of O_3 (ppmv) in equivalent latitude space on the 840 K surface. White solid line represents vortex edge in equivalent latitude.

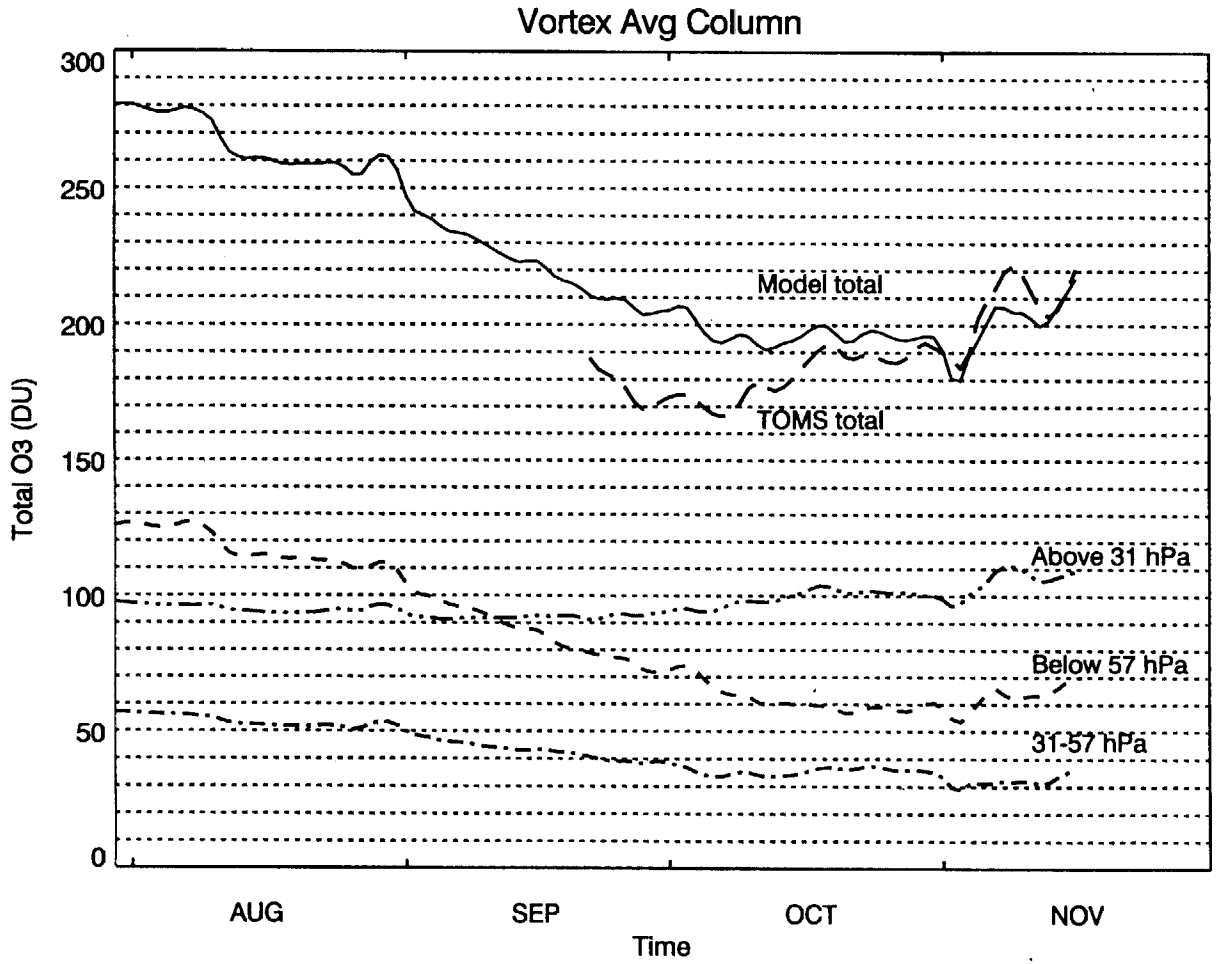
Vortex Avg Column
300
250
200
150
100
50
0
Total O3 (DU)
Model total
TOMS total
Above 31 hPa
Below 57 hPa
31-57 hPa
AUG
SEP
OCT
NOV
Time

Figure 1

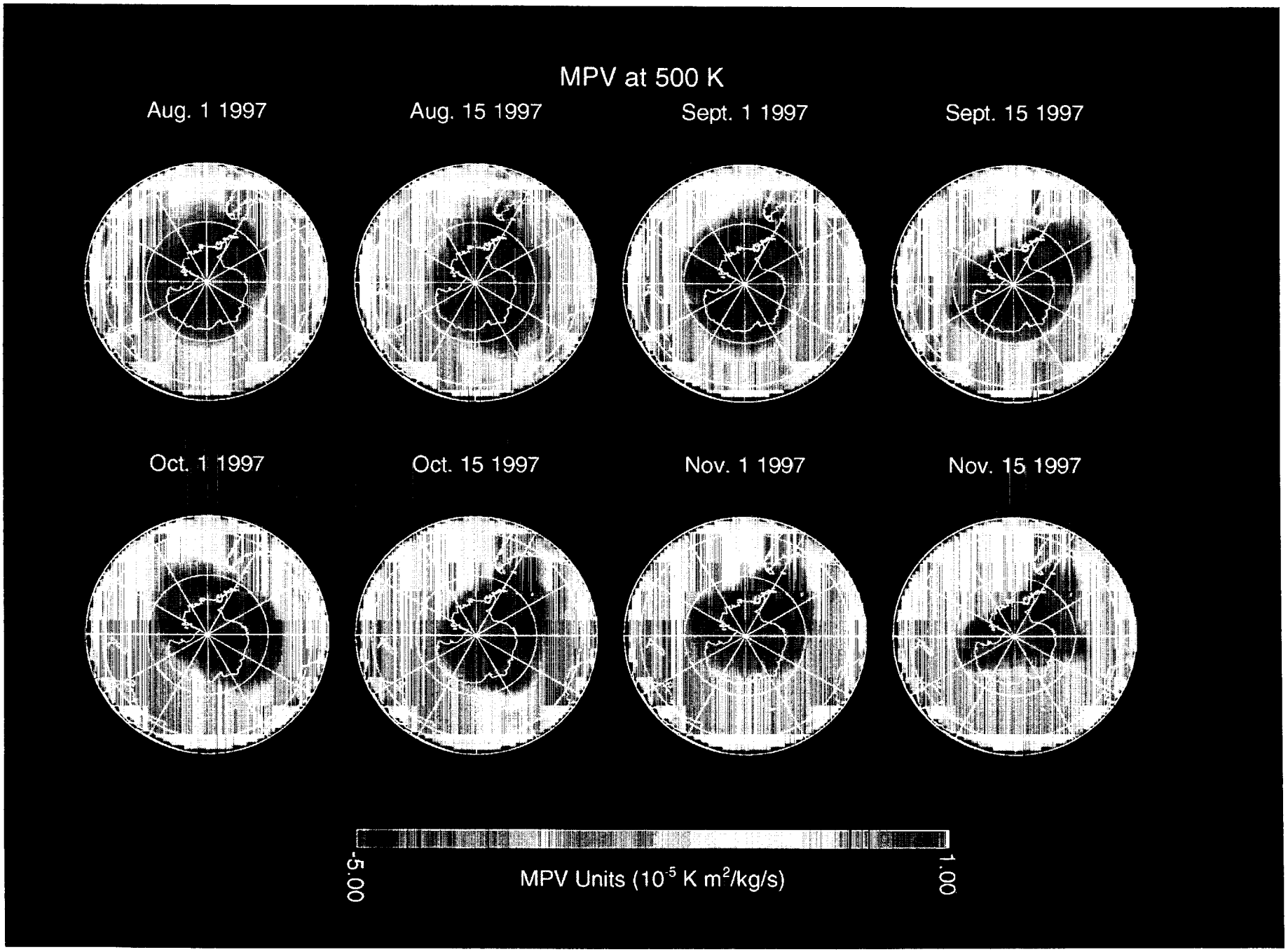
MPV at 500 K
Aug. 1 1997
Aug. 15 1997
Sept. 1 1997
Sept. 15 1997
Oct. 1 1997
Oct. 15 1997
Nov. 1 1997
Nov. 15 1997
-5.00
1.00
MPV Units (10^{-5} K m^2/kg/s)

Figure 2

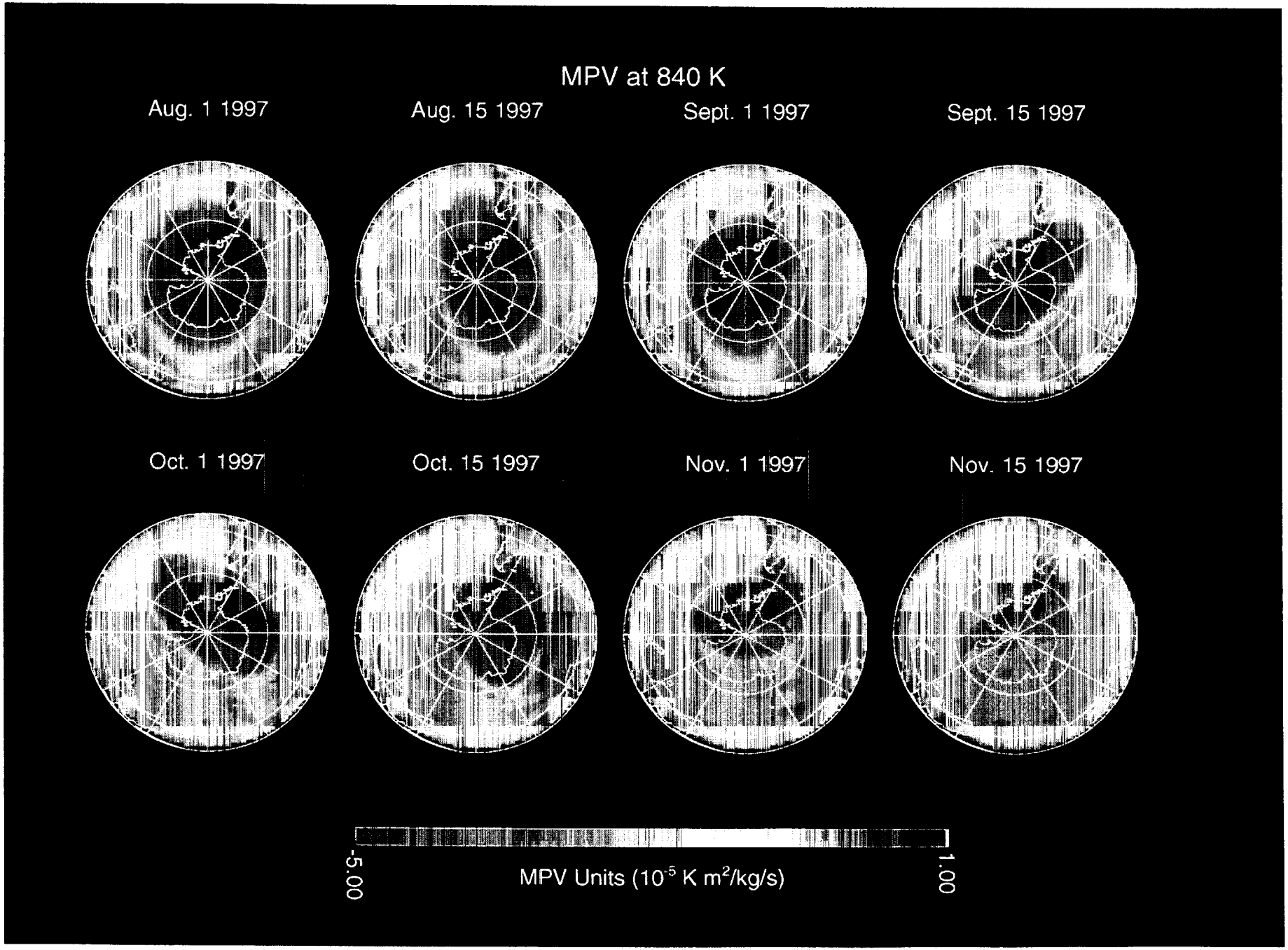
MPV at 840 K
Aug. 1 1997
Aug. 15 1997
Sept. 1 1997
Sept. 15 1997
Oct. 1 1997
Oct. 15 1997
Nov. 1 1997
Nov. 15 1997
-5.00
1.00
MPV Units (10^{-5} K m^2/kg/s)

Figure 3

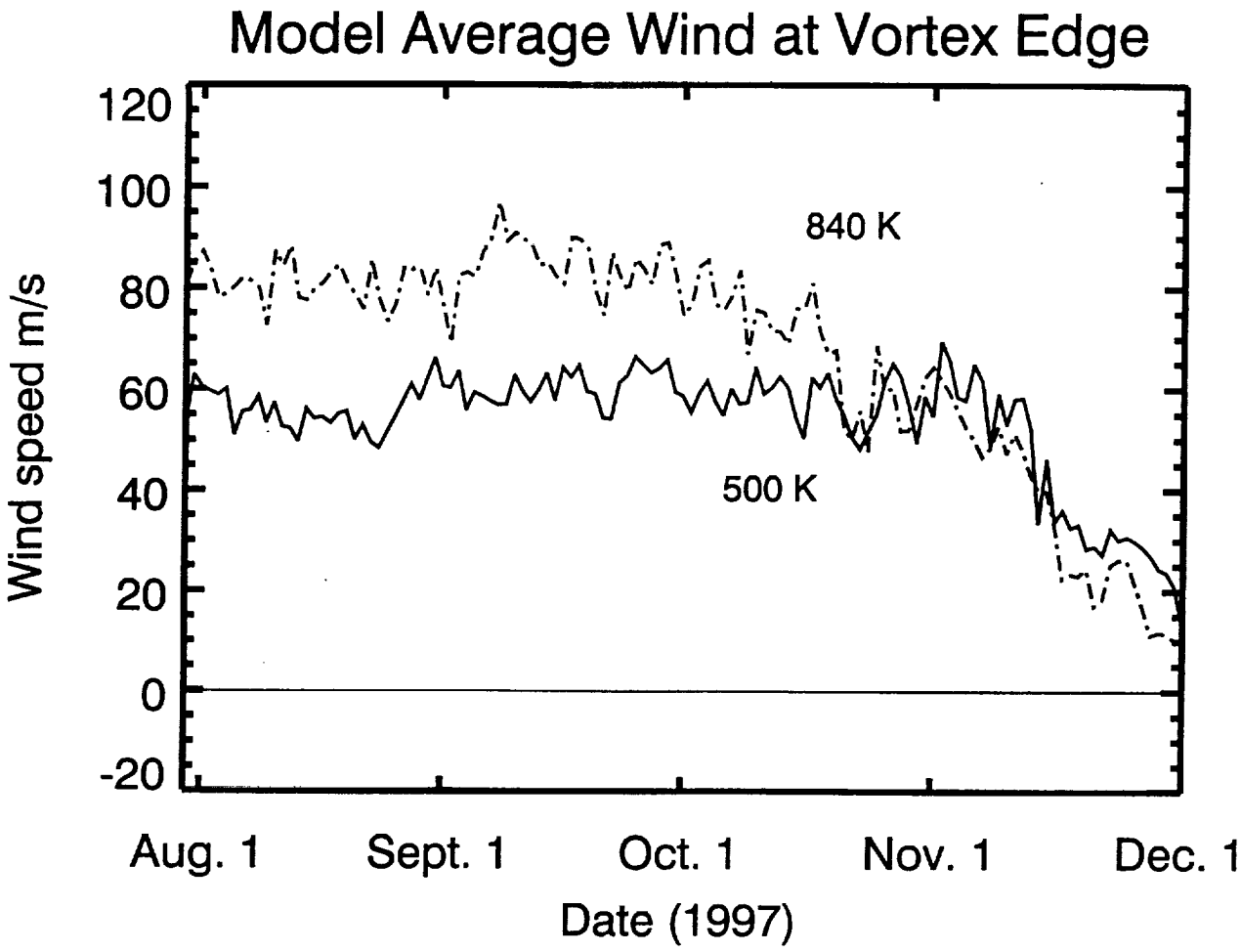
Model Average Wind at Vortex Edge
120
100
80
60
40
20
0
-20
Wind speed m/s
840 K
500 K
Aug. 1
Sept. 1
Oct. 1
Nov. 1
Dec. 1
Date (1997)

Figure 4

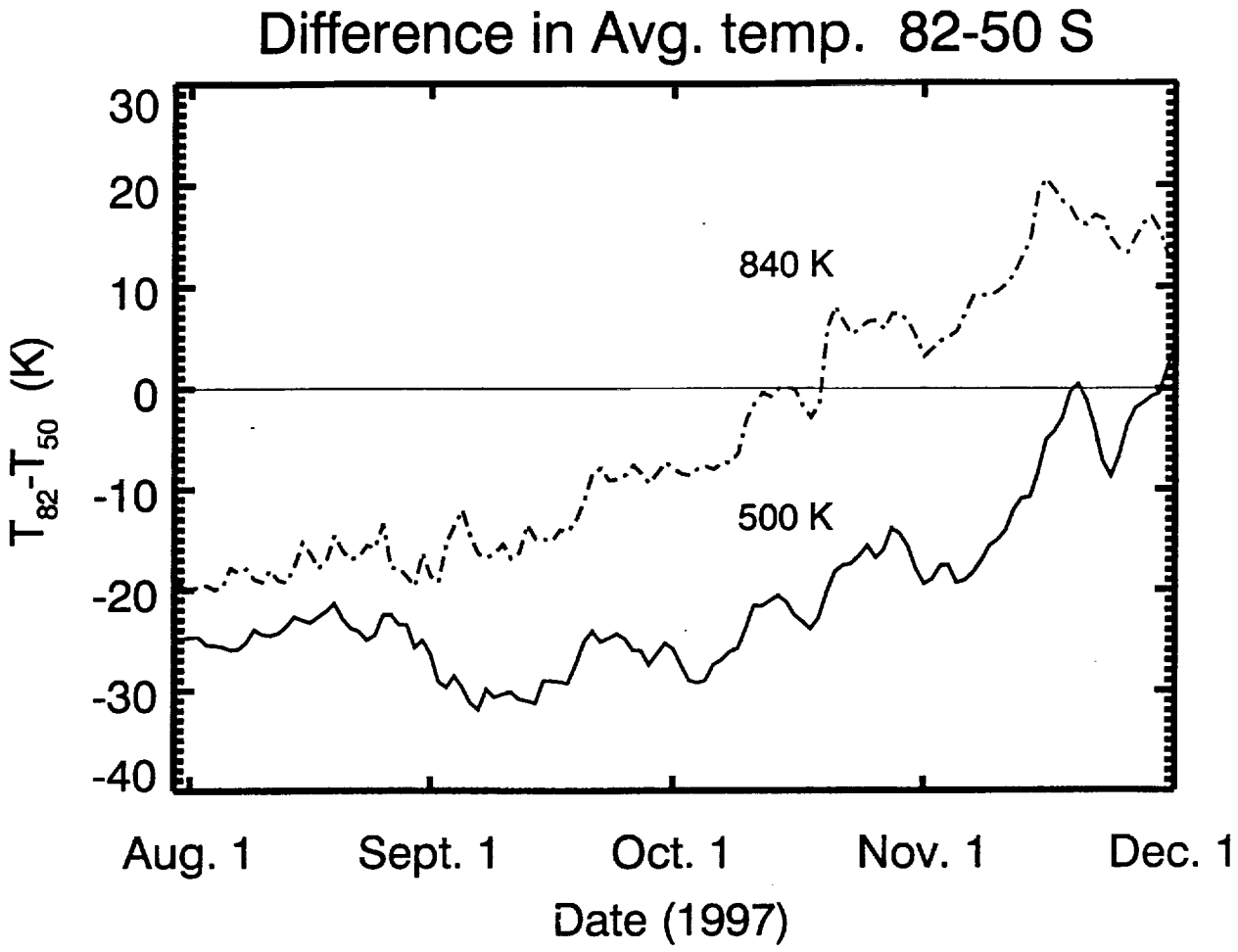
Difference in Avg. temp. 82-50 S
30
20
10
0
-10
-20
-30
-40
T_{82}-T_{50} (K)
840 K
500 K
Aug. 1
Sept. 1
Oct. 1
Nov. 1
Dec. 1
Date (1997)

Figure 5

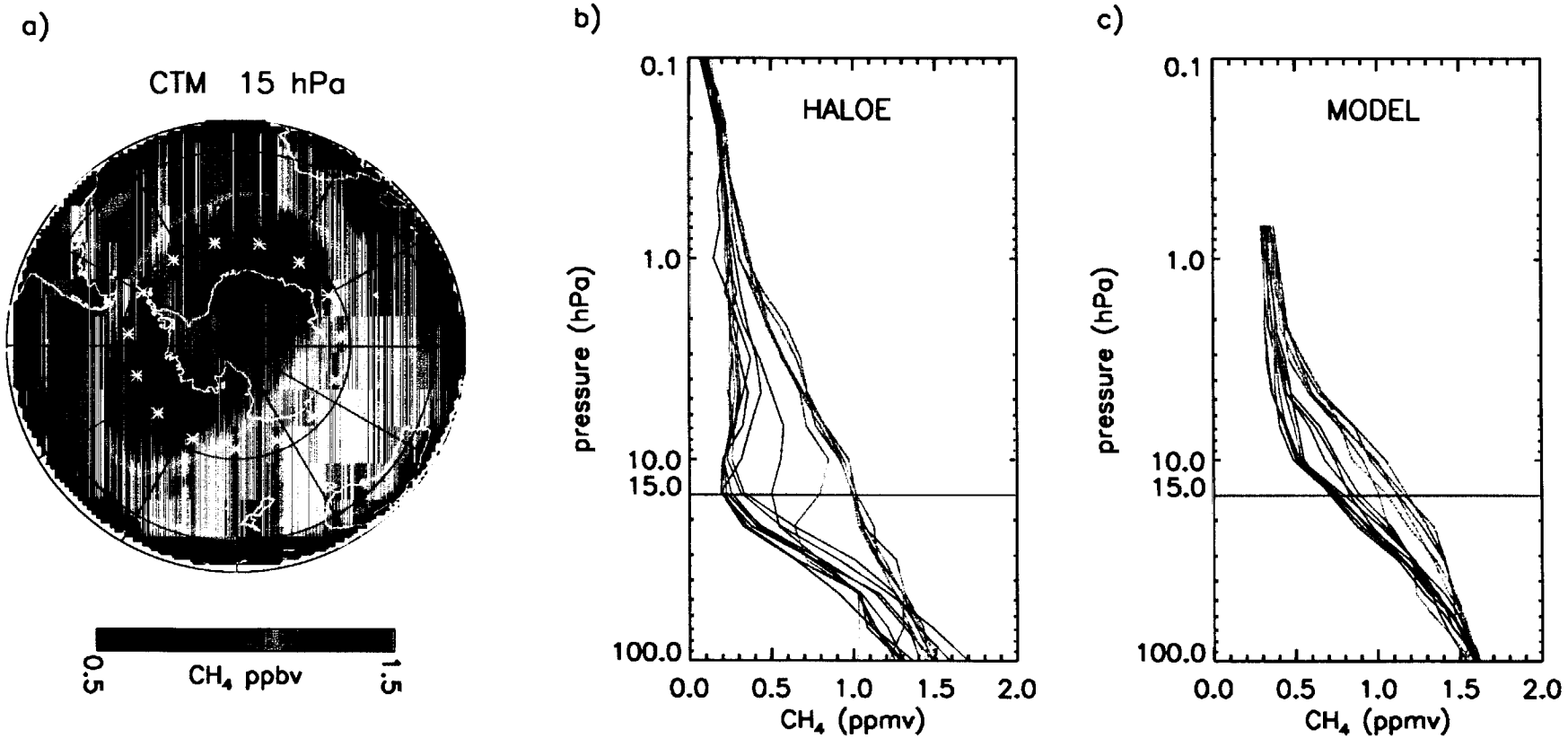
a)
CTM 15 hPa
0.5
CH4 ppbv
1.5
b)
HALOE
pressure (hPa)
0.1
1.0
10.0
15.0
100.0
0.0
0.5
1.0
1.5
2.0
CH4 (ppmv)
c)
MODEL
pressure (hPa)
0.1
1.0
10.0
15.0
100.0
0.0
0.5
1.0
1.5
2.0
CH4 (ppmv)

Figure 6

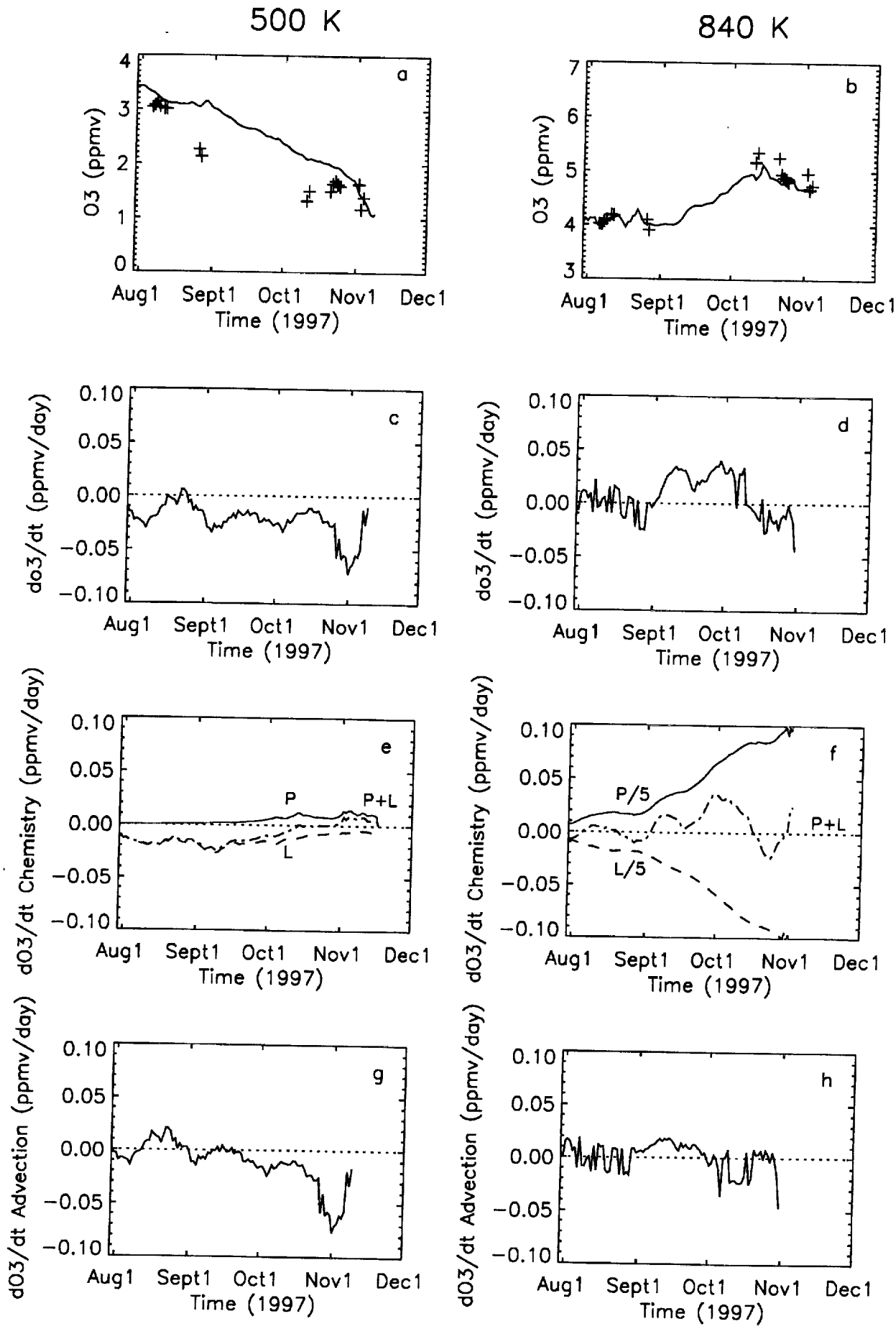
500 K
840 K
a
b
c
d
e
f
g
h
O3 (ppmv)
do3/dt (ppmv/day)
dO3/dt Chemistry (ppmv/day)
dO3/dt Advection (ppmv/day)
P
P+L
L
P/5
L/5
Aug1
Sept1
Oct1
Nov1
Dec1
Time (1997)

Figure 7

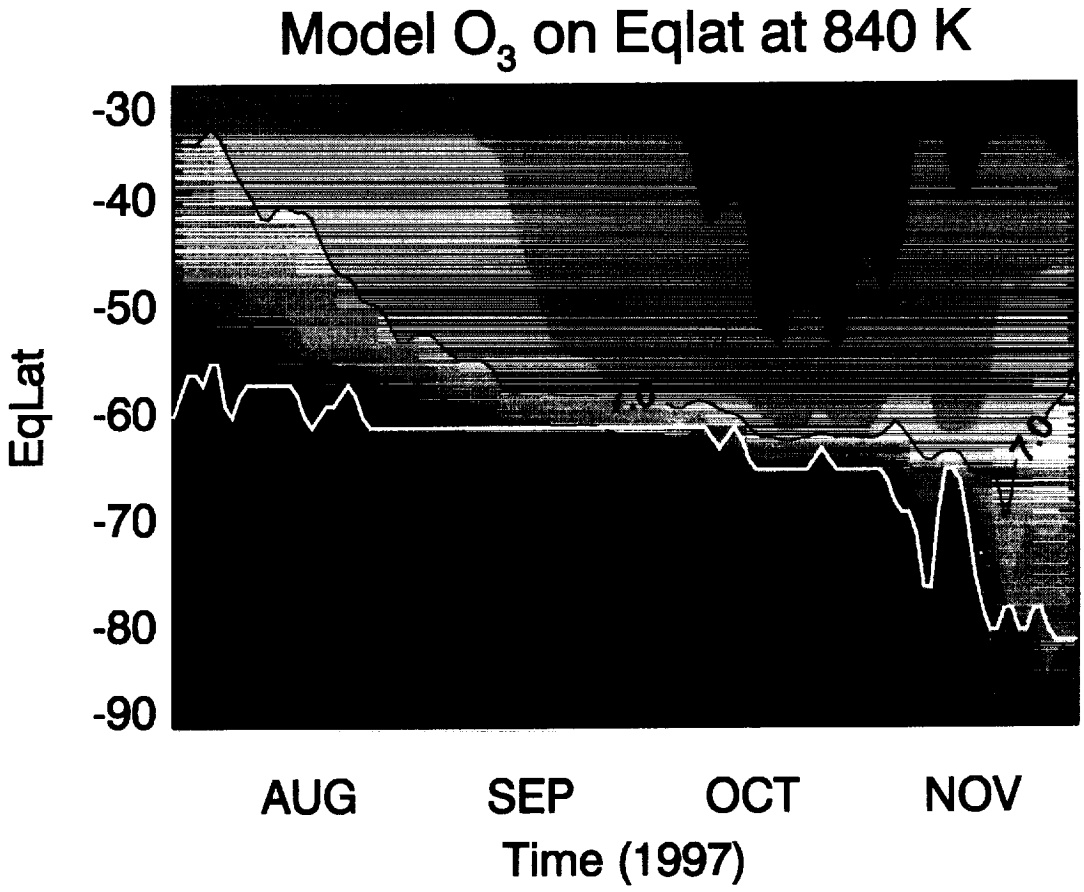
Model O_3 on Eqlat at 840 K
-30
-40
-50
-60
-70
-80
-90
EqLat
AUG
SEP
OCT
NOV
Time (1997)
1.0
1.2

Figure 8